Fast adiabatic control of qubits using optimal windowing theory

John M. Martinis
Department of Physics, University of California, Santa Barbara, CA 93106, USA

Michael R. Geller
Department of Physics and Astronomy, University of Georgia, Athens, Ga 30602, USA

(Dated: February 25, 2014)

A controlled-phase gate was demonstrated in superconducting Xmon transmon qubits with fidelity reaching 99.4%, relying on the adiabatic interaction between the $|11\rangle$ and $|02\rangle$ states. We explain how adiabaticity is achieved even for fast gate times, based on a theory of non-linear mapping of state errors to a power spectral density and use of optimal window functions. With a solution given in the Fourier basis, optimization is shown to be straightforward for practical cases of an arbitrary state change and finite bandwidth of control signals. We find that errors below 10^{-4} are readily achievable for realistic control waveforms.

arXiv:1402.5467v1 [quant-ph] 22 Feb 2014

INTRODUCTION

We recently demonstrated a high fidelity 99.4% [1] controlled-phase gate between two superconducting qubits. High fidelity operation was obtained using the near crossing of the $|11\rangle$ and $|02\rangle$ states, similar to previous work on superconducting qubits [2–4], but now following a new protocol to achieve effective adiabatic behavior with fast gate times. Here we explain how such performance was obtained and give a simple protocol to generate the control waveform for optimum performance.

Achieving fast adiabatic performance is of great interest to the physics community [5–8], with applications in coherent manipulation, precision measurements, and quantum computing . Finding an improved control methodology therefore has wide applications for a variety of quantum systems.

For a two-level quantum system, perfect (transitionless) adiabatic control is possible if control of the σ_y part of the Hamiltonian is accessible, as it is used to cancel non-adiabatic terms coming from changes in σ_x or σ_z [9, 10]. Such "superadiabatic" protocols are not possible here because we consider a system with fixed σ_x and time-dependent σ_z control. Under these conditions, optimized control waveforms have been studied and tested for fast adiabatic changes [11–13], but a general theory of optimized control has not previously been developed. In particular, it is important for quantum computing applications to understand in detail the tradeoff between total control time and state error, and to find waveforms that do not require careful tuning of many parameters.

The set of possible solutions is influenced by other constraints with the superconducting qubit system. Here the non-linearity of the qubits is small [1], so other transitions such as between states $|01\rangle$ and $|10\rangle$ are not far off resonance, giving rise to errors if the control changes too quickly. This requires the system to remain as close to adiabatic as possible throughout the operation, ruling out pulse and refocussing type protocols common in nuclear magnetic resonance [14]. High fidelity thus requires smooth waveforms over the entire time of the control. We also would like to optimize non-standard operations, such as moving into the avoided level crossing regime and then back out to the initial state. Since we are primarily concerned here with errors between the two states $|11\rangle$ and $|02\rangle$ as their frequencies are changed, we may map this to the qubit problem for states $|0\rangle$ and $|1\rangle$ that has a fixed avoided-level crossing (in σ_x) and adjustable qubit frequency (in σ_z).

In this work, we put forward several important insights that allow a physical understanding of adiabatic behavior. We first show how the change in state of a two-level system can be intuitively described in a coordinate system of the instantaneous Hamiltonian. Here, the evolution of the quantum system can be understood in the small error limit using a geometrical construction. Second, the simplicity of this description allows errors to be calculated using a generalized Fourier transform. Third, to obtain a minimum time solution for small changes in angle, the theory of window functions is then used to find optimal control waveforms. We also show that describing the control waveform in a few-term Fourier series is an efficient parameterization of the optimal waveform. We finally show, using a non-linear mapping, how to find the optimal control wavefrom for an arbitrary change in the control Hamiltonian.

These results present a simple yet effective way to optimize for high adiabatic fidelity. We show, perhaps surprisingly, that non-adiabatic errors can be made small even if the interaction time is only slightly larger than the time scale of the transverse coupling, similar to that proposed earlier for a non-adiabatic gate [15].

GEOMETRICAL SOLUTION

We start with a description of a qubit given by the 2-state Hamiltonian

$$H = H_x\sigma_x + H_z\sigma_z = \begin{pmatrix} H_z & H_x \\ H_x & -H_z \end{pmatrix} , \qquad (1)$$

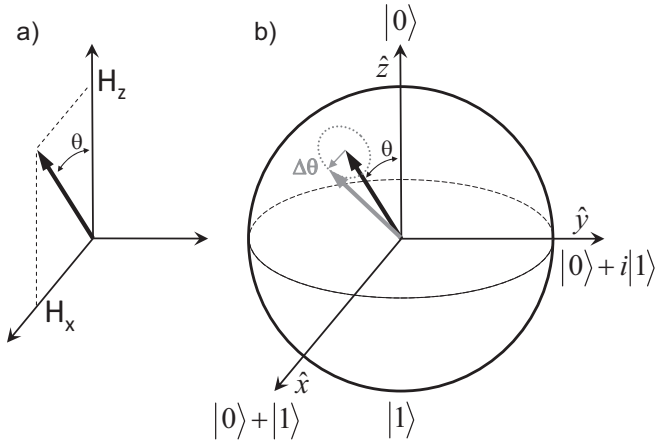

FIG. 1: Geometric picture of non-adiabatic errors. a) Control field of constant H_x and variable $H_z(t)$ gives control angle θ from z-axis. b) Bloch sphere representation gives ground eigenstate parallel to control vector (solid arrow). For a small step in θ, the quantum state (gray arrow) points slightly away, with change $\Delta\theta$ (small gray arrow). This state rotates around eigenstate at frequency ω (gray dotted lines).

where H_x is constant and the qubit frequency is controlled by a time dependent $H_z(t)$, for example the magnetic field in the z-direction for an electron spin. We consider the qubit to be controlled by a Hamiltonian vector $(H_x, 0, H_z)$, having both length and direction. As shown in Fig. 1a, we define the control parameter θ as the angle between the Hamiltonian vector and the z-axis

$$\theta = \arctan(H_x/H_z) \ . \tag{2}$$

The qubit state is described by a Bloch vector that can point in any direction on the Bloch sphere. Here, the usefulness of this geometric construction is the idea that the lowest energy eigenstate has a Bloch vector that points in the direction of the control vector: the eigenstate vector has angle θ from vertical and lies in the plane of the $\hat{x}$ and $\hat{z}$ axes. The ground state eigenvalue $E_- = -\sqrt{H_x^2 + H_z^2}$ is proportional to the length of the control vector, whereas the excited eigenstate points in the opposite direction with eigenenergy $E_+ = -E_-$. If the Bloch state vector is not an eigenstate, then its time dynamics is to rotate (precess) around the eigenstate vector at a frequency proportional to the difference in eigenstate energies

$$\omega = (E_+ - E_-)/\hbar = 2\sqrt{H_x^2 + H_z^2}/\hbar \ . \tag{3}$$

Non-adiabatic errors are typically understood by considering the Landau-Zener trajectory $H_z = \dot{H}_z t$. Initially at large negative times t, where H_z is large and negative, the Hamiltonian control vector points in the down direction, with the state given by the Bloch vector also in the down direction having $\theta = \pi$. As the time goes to zero, the control vector $(H_x, 0, H_z = 0)$ points along the equator, with the Bloch vector $\theta = \pi/2$. At large positive times the control and Bloch vector points in the up direction $\theta = 0$.

When the field is slowly varied ($\dot{H}_z \to 0$), the state adiabatically changes from $\theta = \pi$ to $\theta = 0$. A finite ramp rate gives errors, with the probability to make a transition to the excited final eigenstate as

$$P_e = \exp(-\pi H_x^2/\hbar\dot{H}_z) \ . \tag{4}$$

A small final error $P_e = 10^{-4}$ implies the condition $\dot{H}_z = 0.341\, H_x^2/\hbar$. If we assume a change in H_z from $-10H_x$ to $10H_x$, the total time for the control pulse is $t_c = 18.6\,(h/2H_x)$, where $h/2H_x$ is the oscillation time for the transverse Hamiltonian.

The factor 18.6 implies a long control time for the Landau-Zener trajectory. We will show with optimal control this time factor can be reduced significantly, to order unity.

For adiabatic evolution of the quantum state, the state vector stays aligned with the direction of the control Hamiltonian. To better characterize non-adiabatic errors, we change the reference frame of the Bloch sphere to coincide with that of the control Hamiltonian. In this moving frame $\theta_m = 0$ represents being in the ground state of the instantaneous Hamiltonian, with no non-adiabatic error.

To understand non-adiabatic deviations, we consider the time dynamics of state change. We first consider an infinitesimal time step Δt, during which the the control vector initially changes its direction by $\Delta\theta$, as shown in Fig. 1b. A transformation to the new moving frame produces a small change in the angle of the Bloch vector $-\Delta\theta$. During the remainder of the time Δt the Bloch vector rotates around the $\theta_m = 0$ axis, at the frequency ω. Starting with $\theta_m = 0$ before this time step, the angles θ_x and θ_y in the x- and y-direction can be written compactly as

$$\theta_m \equiv \theta_x + i\theta_y = -\Delta\theta\, e^{-i\omega\Delta t} \tag{5}$$

after time Δt, assuming small angles as appropriate for small non-adiabatic errors. This finite angle implies the quantum state has not changed adiabatically (as $\theta_m \neq 0$), with the error probability given by $P_e = (\sin|\theta_m|/2)^2 \approx |\theta_m|^2/4$.

We next understand the error coming from a sequence of time steps Δt_i each with a small angle change $\Delta\theta_i$. A useful simplification comes from changing to a new frame that rotates with the precession of the Bloch vector, which implies the above θ_m vector does not rotate. Instead, the change $\Delta\theta_i$ rotates in time by an angle ϕ_i, which is computed by summing over all the previous phase changes in the individual steps. The net change in the complex angle of the Bloch vector in this moving

and rotating frame is

$$\theta_{mr} = -\sum_i \Delta\theta_i \, e^{-i\phi_i} \tag{6}$$

$$= -\int dt \, (d\theta/dt) \, \exp[-i \int^t \omega(t')dt'] \, , \tag{7}$$

$$P_e = |\theta_{mr}|^2/4 \, , \tag{8}$$

where P_e is the total probability error. These equations are the general solution for non-adiabatic error in the small error limit.

The amplitude error θ_{mr} is proportional to the rate of change in the eigenstates, as given by $d\theta/dt$. This quantity is mostly averaged to zero because of the rapidly changing phase from the ω integral, with smaller averaged amplitude with increasing qubit frequency ω.

Note that we have assumed here that all changes add linearly. This is a good assumption as long as the net change in angle is very small; for example, it is known that for qubits with small change in state can be approximated by a harmonic oscillator, a linear system. This assumption is generally acceptable since we are only interested in qubit control that give small errors.

An exact calculation of the error, starting from the Schrödinger equation, is derived in Appendix I. It gives results identical to this geometrical solution in the small error limit. There are two changes for the exact solution: the driving amplitude $d\theta/dt$ should also be multiplied by the factor $\cos|\theta_{mr}|$, and the probability is $P_e = \{\sin[\arcsin(\theta_{mr})/2]\}^2$.

To understand how to construct an optimal waveform, we first note that there is a trade-off between the control time and the magnitude of non-adiabatic error. Zero error is not possible - we are instead looking for acceptably small errors, say below 10^{-4}, with as short of a control time as possible. We also want stable control waveforms, so that the error does not increase rapidly for small changes in the waveform.

We first note that non-adiabatic errors are proportional to a change in the control variable θ. Errors will be relatively small when $|H_z| \gg H_x$, due to the slow dependence of θ on H_z/H_x and the large oscillation frequency ω, as described in Eqs. (2) and (3).

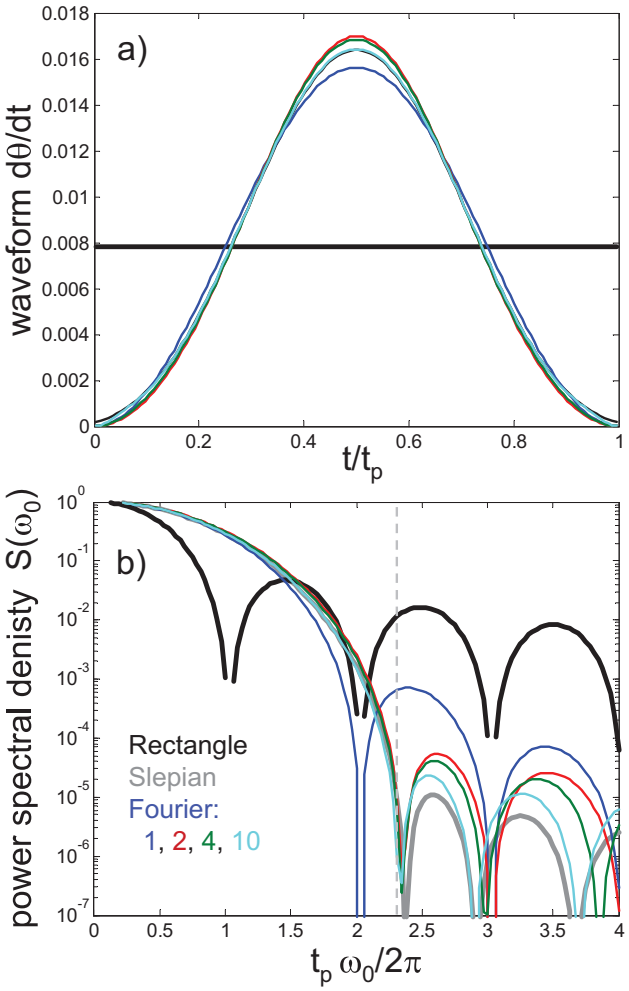

FIG. 2: (color online) Waveform and error for a small change in control θ such that the qubit frequency is constant $\omega = \omega_0$. a) Plot of waveform $d\theta/dt$ versus t/t_p for a rectangular pulse (black), Hanning window (blue), Slepian (gray), and optimized Fourier coefficients with two (red), four (green), and ten (cyan) terms. Note the similarity of the Slepian curves to the optimized Fourier functions, except near $t/t_p = 0, 1$. b) Plot of power spectral density obtained from a Fourier transform of the waveforms in a). All waveforms are normalized to have unit area. The vertical dashed line shows spectral cutoff for minimization of integrated noise.

OPTIMAL SOLUTION: SMALL CHANGE IN θ

For the case where H_z only changes by a small amount, the qubit frequency can be approximated as being constant $\omega = \omega_0$. Then Eq. (7) is just the Fourier transform of $d\theta/dt$ at frequency ω_0, which gives a probability proportional to the power spectral density of the signal at the oscillation frequency ω_0

$$P_e = (1/4) \, S_{d\theta/dt}(\omega_0) \, . \tag{9}$$

This makes sense physically since it is power at the transition frequency, given by $|\theta_{mr}|^2$, that drives the qubit transition to produce errors.

For the simple case of a linear change in the control θ from θ_i to θ_f, the error is proportional to the (constant) derivative $d\theta/dt = (\theta_f - \theta_i)/t_p$, shown as the black line in Fig. 2a. The error versus the pulse time t_p is the power

spectral density of a rectangular pulse

$$P_e^{\rm sq} = (1/4)\Big|(d\theta/dt)\int_0^{t_p} dt\exp(-i\omega_0 t)\Big|^2 \qquad (10)$$

$$= (\theta_f-\theta_i)^2\sin^2(\omega_0 t_p/2)/\omega_0^2 t_p^2\ , \qquad (11)$$

which corresponds to the square of the sinc function. Although the error is zero when $t_p = 2\pi/\omega_0$, small errors occur only around a small range of this time, so we consider this solution not to be stable or practically useful. For large times, the general falloff of the error is quite slow, scaling as $1/t_p^2$, so this control waveform does not present a good solution to adiabatic control.

The functional dependence of the error versus pulse time can be changed by using different control waveforms, which is equivalent to considering different window functions for signal processing [16]. Another example is the function $[1-\cos(2\pi t/t_p)]/2$, known as the Hanning window, as shown in blue in Fig. 2. In this case, the error is

$$P_e^{\rm H} = P_e^{\rm sq}/|1-(\omega_0 t_p/2\pi)^2|^2\ , \qquad (12)$$

where the first zero is at twice the time of the square window $t_p = 4\pi/\omega_0$, but the error falls off more quickly as $1/t_p^6$ at large times. Although this window function is superior to the square window, the errors are still somewhat large right after the first zero, so other window functions should be considered.

From these two examples, it is clear that optimizing non-adiabatic error versus total control time t_p is like optimizing windowing functions: the optimization criteria depend on the requirements for a particular application.

Since we are interested in low errors for a range of pulse times, we define the optimal waveform as one that gives low error for any time larger than some chosen time: this definition is essentially equivalent to adiabatic behavior. We can use the theory of optimal window functions to find this control waveform, known as a Slepian [16]. This function is defined by finding the optimal waveform that minimizes the integrated spectral density above a chosen frequency. For example, the Slepian waveform optimized for frequencies above $\omega_0 t_p/2\pi > 2.3$ is shown in gray in Fig. 2. Although the first minimum is at slightly longer times than for the Hanning window, the error is always below 10^{-5} above this value. A different Slepian cutoff parameter can be used to tradeoff the maximum error for the time of the first minimum.

A disadvantage of the Slepian function is that it does not go to zero at the beginning and end of the pulse, which creates a sharp edge as for a rectangular pulse. This makes the function harder to synthesize, since real waveform generators have finite response times. A practical way around this issue is to find a near optimum solution using Fourier basis functions given by

$$\frac{d\theta}{dt} = \sum_{n=1,2,\ldots,n_m}\lambda_n[1-\cos(2\pi n t/t_p)]\ , \qquad (13)$$

TABLE I: Table of λ_n coefficients obtained from numerical minimization of noise for frequencies $\omega_0 t_p/2\pi > 2.3$, using the constraint $\sum\lambda_n = 1$.

n_m	λ_1	λ_2	λ_3	λ_4	λ_5	λ_6	λ_7
2	1.0866	-0.0866					
4	1.0751	-0.0811	0.0017	0.0044			
10	1.0280	-0.0606	0.0052	0.0055	0.0047	0.0046	0.0035

which goes smoothly to zero at the beginning and end of the pulse. The coefficients are constrained by the height of the pulse

$$\theta_f-\theta_i = t_p\sum_n\lambda_n\ . \qquad (14)$$

Using standard numerical minimization (fminsearch function in MATLAB), the coefficients $\{\lambda_n\}$ can be found that optimizes for the minimum integrated spectral density, as for the Slepian. The waveform and spectral densities for $n_m = 2, 4$, and 10 are plotted in Fig. 2, which shows performance close to the Slepian. Coefficients are given in Table I, showing the first two are dominant. It is particularly interesting to note that the waveform for $n_m = 2$ (red), with only 2 Fourier coefficients, is reasonably close in shape to the Slepian and has acceptably small errors $< 10^{-4}$.

The Fourier basis functions can also include the terms $\lambda_n^s\sin(\pi n t/t_p)$ for n odd, which go to zero at $t = 0, t_p$ but have non-zero derivatives there. Upon using this larger basis set, we find the numerically optimized solutions are not much better than found above only using cosine terms. We choose not use use these sine basis functions because we prefer to also have a zero derivative at the beginning and end of the pulse.

We are also interested in control waveforms that take an initial θ_i to θ_f and then back again to θ_i. In this case the waveform for θ, not $d\theta/dt$, is given by the Fourier basis

$$\theta-\theta_i = \sum_{n=1,2,\ldots,n_m}\lambda_n'[1-\cos(2\pi n t/t_p)]\ , \qquad (15)$$

with constraints on the coefficients

$$\theta_f-\theta_i = 2\sum_{n\ \rm odd}\lambda_n'\ . \qquad (16)$$

The derivative $d\theta/dt$ is now a sum of sine functions, which have non-zero derivatives at the beginning and end of the pulse. Figure 3 shows optimized results for 1, 2, and 3 Fourier coefficients, as well as for the first-harmonic solution of the Slepian. As for the previous case, the optimized Fourier solution is close to that of the Slepian: only two coefficients (red curve) is required for close approximation to the ideal solution.

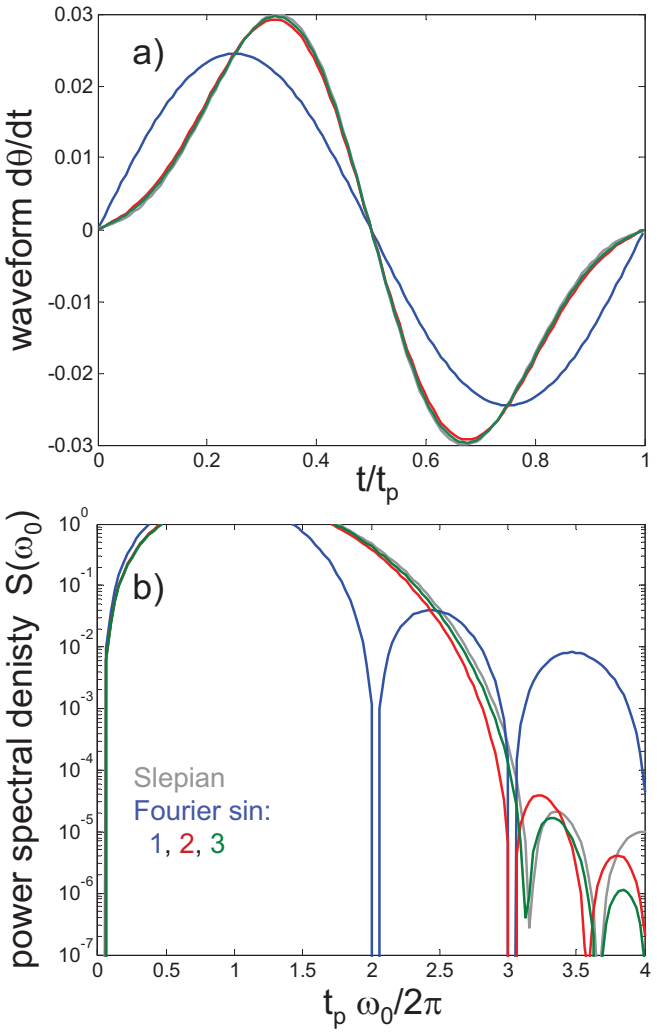

FIG. 3: (color online) Waveform and error as for Fig. 2, but going from θ_i to θ_f and back. a) Plot of waveform $d\theta/dt$ versus t/t_p for optimized Fourier coefficients with one (blue), two (red), and three (green) terms, as well as Slepian (gray). b) Plot of power spectral density from Fourier transforms of the waveforms in a). Waveforms normalized using $2\sum \lambda'_n = 1$.

OPTIMUM SOLUTION: ARBITRARY θ

The optimal solution for an arbitrary change in θ will have to account for the qubit frequency ω changing during the control pulse. The solution is found by first making a coordinate transformation to an accelerating frame in time where the oscillation frequency is constant, and then using optimal waveforms as found previously.

The basic idea is to define a new frame with time τ such that the rate of change of the phase is constant. Choosing this frequency as the constant $\omega_x = 2H_x/\hbar$, the times are related by

$$\omega_x \, d\tau = \omega(t) \, dt \ . \tag{17}$$

In this frame, the error angle from Eq. (7) becomes

$$\theta_{mr} = -\int d\tau \, (d\theta/d\tau) \, \exp[-i\omega_x \tau] \ , \tag{18}$$

so that the optimal shape of $d\theta(\tau)/d\tau$ can be computed for constant frequency ω_x, as done in the last section. Integration of $d\theta/d\tau$ is next used to compute the quantity $\theta(\tau)$. The relationship between the real time t and τ is finally solved by integrating Eq. (17)

$$t(\tau) = \int^{\tau} d\tau' \, \omega_x/\omega(\tau') \tag{19}$$

$$= \int^{\tau} d\tau' \, \sin\theta(\tau') \ , \tag{20}$$

where in the last equation we have used Eqs. (2) and (3) to find the relation $\omega = \omega_x/\sin\theta$. The function $t(\tau)$ can be inverted numerically using interpolation. For example, in MATLAB code the dependence $\theta(t)$ would be given through the interpolation of the vectors $t(\tau)$ and $\theta(\tau)$ using the command $\theta(t) =$interp1$(t(\tau), \theta(\tau), t)$.

To illustrate this solution for an arbitrary control problem, we first consider the avoided level crossing from $H_z = -10H_x$ to $H_z = 10H_x$, as discussed earlier for the Landau-Zener trajectory. The waveform is shown as solid lines in Fig. 4a for the 2 Fourier coefficients $\{\lambda_1 = 1.086, \lambda_2 = -0.086\}$ found earlier. Here we find the control waveform is nearly linear in θ, not in H_z as assumed for the standard Landau-Zener problem. The non-adiabatic error P_e is plotted in Fig. 4b, both for the linearized (black) and the exact (blue) solution of the qubit dynamics. The linearized solution has similar shape to that found earlier, as expected, whereas the exact solution shows significantly higher errors, demonstrating that an exact solution for this control problem is important.

To further reduce error, we next optimize the λ_n coefficients for better performance. Shown in green is the best performance obtained for varying λ_2, whereas the red curve shows optimal performance for a choice of λ_2 and λ_3. It is impressive that non-adiabatic errors in the 10^{-5} range can be obtained with only a small number of coefficients. Also note that that low errors occurs at a pulse time t_p equal to one oscillation period $h/2H_x$ of the avoided level crossing, about 20 times faster than the simple Landau-Zener trajectory.

Another important waveform is for a controlled pulse in θ, as shown earlier in Fig. 3. Here we consider the control angle changing from $\theta_i = 10H_x$ to $\theta_f = 0.55\,\pi/2$, then back again to θ_i, which corresponds to the adiabatic controlled-phase gate for two qubits using the states $|11\rangle$ and $|02\rangle$. In this case $\theta(\tau)$ is given by Eqs. (15) and (16), and $\theta(t)$ is found as for the last example. We find a near optimal solution for only one additional coefficient $\lambda'_2 = -0.19$, as shown in black in Fig. 5. We obtain very low error for a total control time about one oscillation of $\omega_x/2\pi$.

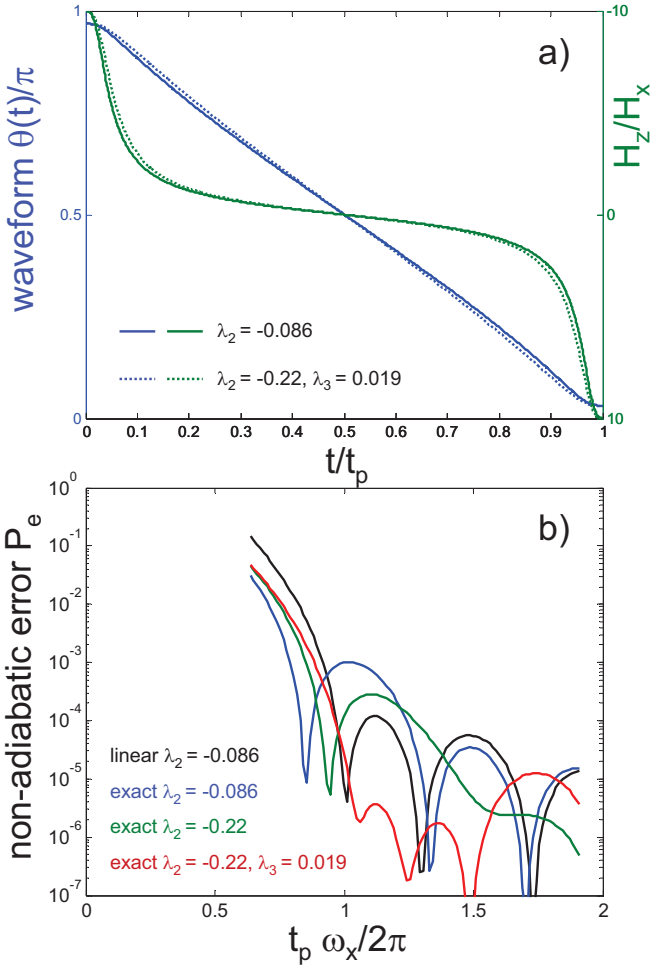

FIG. 4: (color online) Waveform and error for H_z changing from $-10H_x$ to $10H_x$. a) Blue lines are plot of control $\theta(t)$ versus t/t_p for two (solid) and three (dashed) Fourier coefficients. The right scale shows the waveform $H_z(t)$ as green lines. b) Plot of non-adiabatic error versus pulse time t_p for linearized and exact solutions, with both two and three optimized coefficients. Low errors can be achieved for times greater than $t_p = 2\pi/\omega_x$, corresponding to one oscillation at the avoided level crossing. We define $\omega_x = 2H_x/\hbar$.

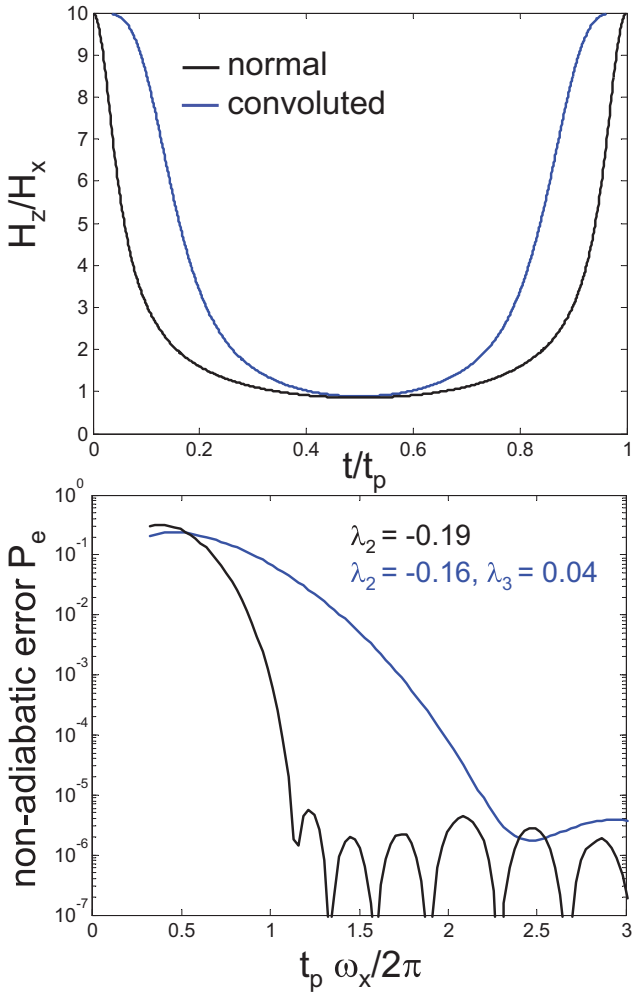

FIG. 5: (color online) Waveform and error for H_z changing from $10\,H_x$ to $1.17\,H_x$, and then back to $10H_x$. a) Black line is for optimal waveform, whereas blue line includes the effect of waveform rounding by control electronics, here accounted for by a convolution. Optimal coefficients are $\{\lambda_2', \lambda_3'\} = \{-0.19, 0\}$ for black and $\{-0.16, 0.04\}$ for blue line. b) Plot of non-adiabatic error versus pulse time t_p for the two cases.

This waveform requires fast changes in H_x at the beginning and end of the pulse. Because of the finite bandwidth of the control electronics, such a shape may not be possible to synthesize, so we next consider the optimal control including rounding of the waveform, here accounted for by convolution of the output waveform with a Gaussian. With convolution, the computed non-adiabatic error increases significantly with the original λ_2' coefficient. We found that adjusting λ_2' could not improve the error much, but by including the next coefficient λ_3' the error could be effectively minimized. This optimal solution is shown as the blue line in Fig. 5, where low error is now found at about twice the oscillation period of $\omega_x/2\pi$. Note that about 1/2 of the increase in time of the control waveform is accounted for by the extra time added at the beginning and end of the pulse from convolution.

OPTIMUM SOLUTION FOR 2 STATE ERRORS

The Fourier basis may be used to optimize waveforms for other control problems, such as minimizing the excitation to the 2nd excited state when driving weakly anharmonic qubits. For a qubit anharmonicity $A/2\pi$, Fig. 6 shows the average 2 state error versus pulse time for a π-pulse. The black curve is for the optimal case only including a λ_2 coefficient in the control waveform. We find a much better solution using Derivative Removal

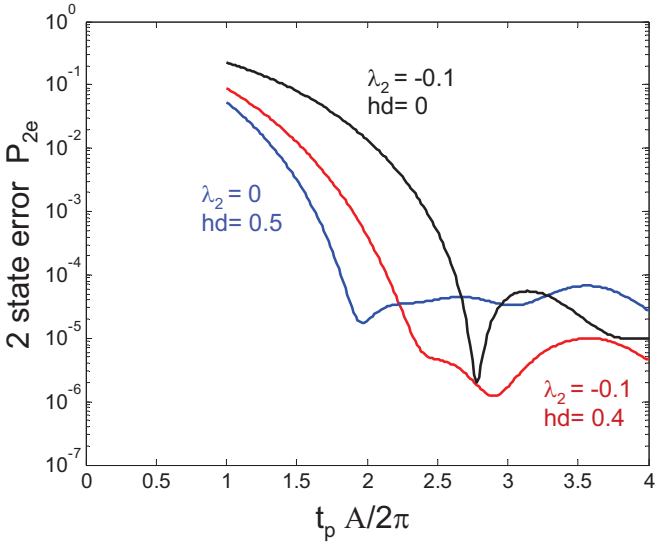

FIG. 6: (color online) Average probability of a two-state error versus pulse time for a qubit π-pulse. The time is normalized with the qubit non-linearity $A/2\pi$. The black curve is for an optimized $\lambda_2 = -0.1$ using no half-derivative term $hd = 0$. The blue curve is using $hd = 0.5$, whereas the red is optimized to give errors below 10^{-5}.

by Adiabatic Gate (DRAG) [17] when including a half-derivative term ($hd = 0.5$) [18], as shown in blue. A lower error, albeit slightly longer pulse time, is shown for the red curve which optimizes both hd and λ_2. Here, the error is taken as the average of the squared unitary elements $0 \to 2$ and $1 \to 2$ in the transformation matrix, solved for a π pulse on the qubit states.

CONCLUSION

We have shown that an optimal control waveform for adiabatic behavior may be obtained by minimizing the spectral weight integrated above a cutoff frequency. Although the best solution is a Slepian, optimization of a few-term Fourier series shows comparably low errors, with acceptable performance achieved with only two or three coefficients. This solution can be used for arbitrary control, even when the transition frequency is changing in time, by first solving the problem with a fixed frequency and then transforming to the proper time frame. We find effects of finite bandwidth in the control waveform can be readily accounted for by optimizing the Fourier coefficients. This method of solution can be used for other control problems, such as minimizing the 2-state occupation for a single qubit π-pulse.

With this protocol, we find that gates with intrinsic error below 10^{-4} should be possible for the two-qubit controlled-phase operation, even for relatively fast gate times. This theoretical understanding may open up a new route to ultra-high fidelity quantum operations and fault tolerant quantum computation.

We thank A. Korotkov for helpful discussions. This work was supported by the Office of the Director of National Intelligence (ODNI), Intelligence Advanced Research Projects Activity (IARPA), through the Army Research Office grants W911NF-09-1-0375 and W911NF-10-1-0334. All statements of fact, opinion or conclusions contained herein are those of the authors and should not be construed as representing the official views or policies of IARPA, the ODNI, or the U.S. Government.

APPENDIX I: EXACT SOLUTION

The exact quantum solution to the non-adiabatic problem may be expressed in the form found geometrically. We start by considering the effect of a rotation around the H_x-axis. If the wavefunction in a fixed basis is given by $|\Psi\rangle = a|0\rangle + b|1\rangle$, then it can be rewritten in a basis rotated by the angle θ as $|\Psi\rangle = \alpha|-\rangle + \beta|+\rangle$, re-expressed in eigenstates of the new basis with amplitudes given by

$$\alpha = a\cos(\theta/2) - b\sin(\theta/2)\ , \tag{21}$$
$$\beta = b\cos(\theta/2) + a\sin(\theta/2)\ . \tag{22}$$

In the θ-rotated basis we define the energy eigenvalues as $\pm\omega/2$, which introduces phase factors that has differential form $\dot\alpha = -i(\omega/2)\alpha$ and $\dot\beta = i(\omega/2)\beta$. We are interested in changes in the control vector, so if θ changes with time one finds

$$\dot\alpha = -i(\omega/2)\alpha - a\sin(\theta/2)\,\dot\theta/2 - b\cos(\theta/2)\,\dot\theta/2 \tag{23}$$
$$= (-i\omega\alpha - \dot\theta\beta)/2\ , \tag{24}$$
$$\dot\beta = (+i\omega\beta + \dot\theta\alpha)/2\ . \tag{25}$$

Note the symmetry of the rotations, with factors $i\omega$ for the time-dependence of H_z rotations, and $\dot\theta$ for the H_x rotation.

The time dependence can be described simply if one considers the quantity $\alpha^*\beta$, where * is the complex conjugate. Its derivative is

$$\frac{d}{dt}(\alpha^*\beta) = (i\omega\alpha^* - \beta^*\dot\theta)\beta/2 + \alpha^*(i\omega\beta + \alpha\dot\theta)/2] \tag{26}$$
$$= i\omega(\alpha^*\beta) + (|\alpha|^2 - |\beta|^2)\dot\theta/2 \tag{27}$$
$$= i\omega(\alpha^*\beta) + \sqrt{1 - 4|\alpha^*\beta|^2}\ \dot\theta/2\ , \tag{28}$$

where in the last equation we have used the relation

$$\left(|\alpha|^2 - |\beta|^2\right)^2 = |\alpha|^4 + 2|\alpha|^2|\beta|^2 + |\beta|^4 - 4|\alpha^*\beta|^2 \tag{29}$$
$$= \left(|\alpha|^2 + |\beta|^2\right)^2 - 4|\alpha^*\beta|^2 \tag{30}$$
$$= 1 - 4|\alpha^*\beta|^2\ . \tag{31}$$

Note that the square root factor in Eq. (28) changes sign when $|\alpha|^2 - |\beta|^2$ is negative.

For Bloch vector angles Θ and φ the amplitudes are $\alpha = \cos(\Theta/2)$ and $\beta = \sin(\Theta/2)e^{i\varphi}$, which gives

$$\alpha^*\beta = \cos(\Theta/2)\sin(\Theta/2)e^{i\varphi} \quad (32)$$

$$= \sin\Theta\, e^{i\varphi}/2\ . \quad (33)$$

so that its magnitude is the error probability $P_e = [\sin(\Theta/2)]^2 \approx |\alpha^*\beta|$ only for small angles Θ. Inserting this result for $\alpha^*\beta$ into Eq. (28), one finds

$$\frac{d}{dt}(\sin\Theta\, e^{i\varphi}) = i\omega(\sin\Theta\, e^{i\varphi}) + \cos\Theta\ \dot{\theta}\ . \quad (34)$$

Changing phase variables $\varphi = \varphi' + \phi$, where $\phi = \int \omega dt$ and noting that $d\phi/dt = \omega$, we can remove the $i\omega$ phase term

$$\frac{d}{dt}(\sin\Theta\, e^{i\varphi'}) = \cos\Theta\ \dot{\theta}e^{-i\phi}\ , \quad (35)$$

which is equivalent to previous geometrical result Eq. (7) in the low amplitude limit $\Theta \to 0$. Here, the exact solution has the amplitude of the drive term $d\theta/dt$ rescaled by $\cos\Theta$ to account for the geometry of the Bloch sphere.

[1] R. Barends, J. Kelly, A. Megrant, A. Veitia, D. Sank, E. Jeffrey, T. C. White, J. Mutus, A. G. Fowler, B. Campbell, Y. Chen, Z. Chen, B. Chiaro, A. Dunsworth, C. Neill, P. O'Malley, P. Roushan, A. Vainsencher, J. Wenner, A. N. Korotkov, A. N. Cleland, and John M. Martinis, arXiv:1402.4848.

[2] F. W. Strauch, P. R. Johnson, A. J. Dragt, C. J. Lobb, J. R. Anderson, and F. C. Wellstood, Phys. Rev. Lett. **91**, 167005 (2003).

[3] L. DiCarlo, M. D. Reed, L. Sun, B. R. Johnson, J. M. Chow, J. M. Gambetta, L. Frunzio, S. M. Girvin, M. H. Devoret, and R. J. Schoelkopf, Nature **467**, 574 (2010).

[4] T. Yamamoto, M. Neeley, E. Lucero, R. C. Bialczak, J. Kelly, M. Lenander, Matteo Mariantoni, A. D. O'Connell, D. Sank, H. Wang, M. Weides, J. Wenner, Y. Yin, A. N. Cleland, and John M. Martinis, Phys Rev. **B 82**, 184515 (2010).

[5] G. Schaller, S. Mostame and R. Schutzhold, Phys. Rev. **A 73**, 062307 (2006)

[6] D. A. Garanin and R. Schilling, Europhys. Lett. **59**, 7 (2002).

[7] D. A. Garanin and R. Schilling, Phys. Rev. **B 66**, 174438 (2002).

[8] E. Torrontegui, S. Ibáñez, S. Martí nez-Garaot, M. Modugno, A. del Campo, D. Guéry-Odelin, A. Ruschhaupt, Xi Chen, J. G. Muga, arXiv:1212.6343v1 [quant-ph].

[9] R. Lim and M.V. Berry, J. Phys. A: Math. Gen. **24**, 3255 (1991).

[10] M.V. Berry, J. Phys. A: Math. Theor. **42** 365303 (2009).

[11] M. G. Bason, M. Viteau, N. Malossi, P. Huillery, E. Arimondo, D. Ciampini, R. Fazio, V. Giovannetti, R. Mannella, and O. Morsch, Nature Physics **8**, 147 (2012).

[12] J. Roland and N. J. Cerf, Phys. Rev. **A 65**, 042308 (2002).

[13] X. Cao, J. Zhuang, Z.-J. Ning and W. Zhang, arXiv:1201.1962v1 [quant-ph].

[14] A. Mitra, A.Ghosh, R. Das, A. Patel, A. Kumar, J. Mag. Res. **177**, 285 (2005).

[15] J. Ghosh, A. Galiautdinov, Z. Zhou, A. N. Korotkov, J. M. Martinis, and M. R. Geller, Phys. Rev. **A 87**, 022309 (2013).

[16] W.H. Press, S. A. Teukolsky, W. T. Vetterling, and B. P. Flannery, *Numerical Recipes 3rd Edition: The Art of Scientific Computing*, (New York: Cambridge University Press 2007).

[17] F. Motzoi, J.M. Gambetta, P. Rebentrost, and F.K. Wilhelm, Phys. Rev. Lett. **103**, 110501 (2009).

[18] E. Lucero, J. Kelly, R. C. Bialczak, M. Lenander, M. Mariantoni, M. Neeley, A. D. O'Connell, D. Sank, H. Wang, M. Weides, J. Wenner, T. Yamamoto, A. N. Cleland, J. M. Martinis, Phys. Rev. **A 82**, 042339 (2010).